Experiments to Simulate Effect of Marangoni Convection on Weld Pool Shape

At high Peclet numbers, the pool bottom can be flat or even convex instead of concave

BY C. LIMMANEEVICHITR AND S. KOU

ABSTRACT. Stationary welds of sodium nitrate ($NaNO_3$, a high-Prandtl-number material) and gallium (Ga, a low-melting-point, low-Prandtl-number material) were made with a defocused CO_2 laser beam to simulate the effect of Marangoni convection on the shape of arc weld pools *without* a surface-active agent. A Peclet number representing the ratio of (heat transport by convection)/(heat transport by conduction) was defined as Pe = LV/α, where L is the pool surface radius, V the maximum *outward* surface velocity and α the thermal diffusivity. The Ga and $NaNO_3$ pools represented the low and high extremes of Pe, respectively, with commonly welded metals such as aluminum, steel and stainless steel falling in between. By going to these extremes, the effect of convection on the pool shape could be much more easily understood. For Ga, Pe was low because low V (weak Marangoni convection) and high α promoted conduction down into the pool, and the resultant pool bottom was concave. For $NaNO_3$, however, Pe became high easily because high V (strong Marangoni convection) and very low α promoted outward convective heat transport, and the resultant pool bottom was shallow and flat. Reducing the beam diameter further increased V (even stronger Marangoni convection) and Pe. The fast outward surface flow turned and penetrated downward at the pool edge, resulting in a convex pool bottom. Both the flat and convex pool bottoms are a clear indication Marangoni convection dominated over gravity-induced buoyancy convection. It is proposed that, in the absence of both a surface-active agent and a significant electromagnetic force, the pool bottom convexity increases with increasing Pe. It was shown that, for a given material composition and welding process, the weld shape often reveals a good deal about the nature of weld pool convection.

C. LIMMANEEVICHITR and S. KOU are graduate student and Professor, respectively, in the Department of Materials Science and Engineering, University of Wisconsin, Madison, Wis.

Introduction

Marangoni convection, also called surface-tension-driven convection or thermocapillary convection, can affect the shape of the weld pool dramatically (Ref. 1). Unfortunately, it has not been revealed clearly either in a real or simulated weld pool. The effect of Marangoni convection on the weld pool shape can be studied much better if the disturbance from the electromagnetic force of the arc can be avoided and if convection can be visualized.

Ishizaki, *et al.* (Ref. 2), observed Marangoni convection in a thin slice of molten paraffin heated by a soldering iron in contact with its top surface, *i.e.*, Marangoni convection was two dimensional rather than axisymmetrical like in a stationary weld pool. Unlike $NaNO_3$, paraffin is often a mixture of several organic compounds, and the physical properties are not well defined. Furthermore, contact between a heater of even a very small size and the free surface causes significant distortions of the free surface and the flow pattern, as shown in a recent study by the authors (Ref. 3).

In that study (Ref. 3), physical simulation of Marangoni convection in weld pools without a surface-active agent was conducted. Marangoni convection in a simulated transparent weld pool of $NaNO_3$ 10 mm in diameter was induced by a defocused CO_2 laser beam as the heat source and revealed by flow visualization with a laser light-cut technique for illumination. No contact existed between the pool surface and any heater such as a soldering iron. The observed Marangoni convection was expected to resemble that in welding because the Marangoni number was close to those in welding, according to the similarity law of hydrodynamics.

KEY WORDS

Electron Beam Welding
Gas Tungsten Arc Welding
Laser Beam Welding
Marangoni Convection
$NaNO_3$
Peclet Number
Prandtl Number
Weld Pool Shape

For convenience of discussion, a typical flow pattern is shown in Fig. 1A. Two counterrotating cells are present in the meridian plane of the pool, the outward surface flow is much faster than the inward return flow and the centers of the cells are near the pool edge. Increasing the beam power (0.5 to 5.4 W) and reducing the beam diameter (5.9 to 1.5 mm) both cause Marangoni convection to become faster. The latter, however, has a significantly greater effect; the surface flow is so much stronger as to force the return flow to penetrate deeper into the pool, as illustrated in Fig. 1B. This penetrating return flow has a rather significant effect on the weld pool shape, as will be described in the following pages.

One purpose of the present investigation is to study the effect of Marangoni convection on the weld pool shape in light of the flow visualization experiments (Ref. 3). Another purpose is to relate the weld pool shape to the Peclet number and the Prandtl number.

Experimental Procedure

Materials and Sample Preparation

$NaNO_3$ and Ga were selected for welding because they represent the two extremes of high- and low-Prandtl-number materials, respectively. The Prandtl number is defined as Pr = $C_p\mu/k$, where C_p is the specific heat, μ is the dynamic viscosity and k is the thermal conductivity. In other words, the lower the thermal conductivity, the higher the Pr. For $NaNO_3$, Pr = 9.12, and, for Ga, Pr = 0.0234. Most commonly welded metals have a Pr between these two numbers; Pr is about 0.02 for aluminum, 0.08 for steel and 0.16 for stainless steel. As will be described later, $NaNO_3$ pools and Ga pools also represent the high and low extremes

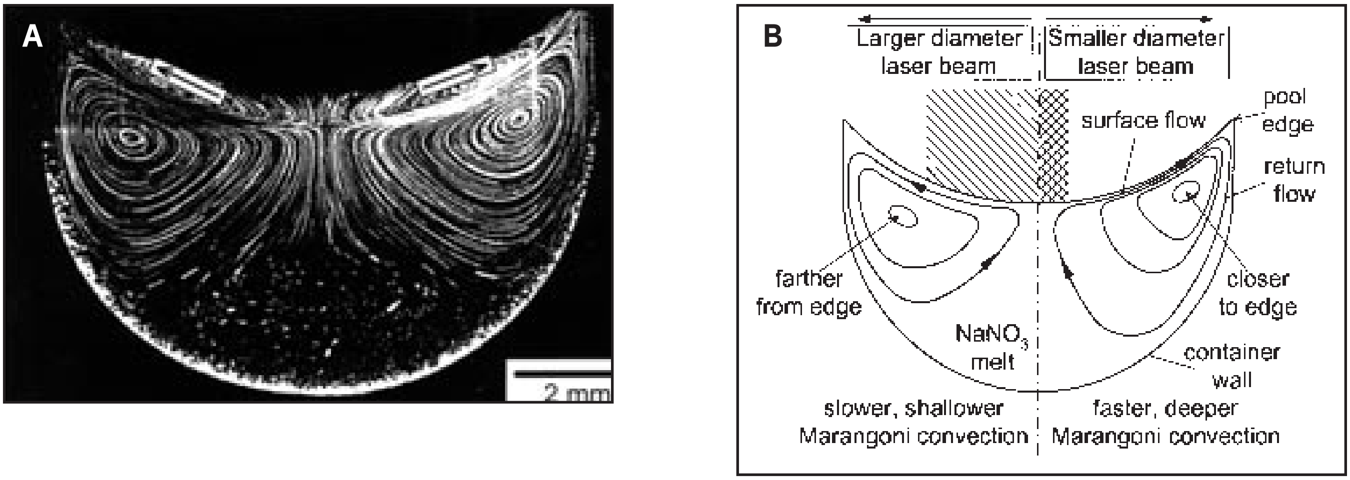

Fig. 1 — Marangoni convection in a simulated weld pool of $NaNO_3$ 10 mm in diameter. A — flow pattern induced by a 2.5-W CO_2 laser beam 3.2 mm in diameter (Ref. 3); B — effect of beam diameter on convection pattern under a constant power.

of the Peclet number, respectively, with weld pools of most commonly welded materials in between the two. By going to these extremes of the Prandtl and Peclet numbers, the effect of material properties and weld pool convection on the weld pool shape could be much more easily seen and understood.

Another reason for selecting $NaNO_3$ was because it had been used recently for flow visualization of Marangoni convection (Ref. 3). Its physical properties (Refs. 4–6) are listed in Table 1. $NaNO_3$ has a transmission range 0.35 to 3 µm (Ref. 7) and is, therefore, opaque to a CO_2 laser beam (10.6 µm), just as a weld pool is opaque to the heat source. The purity of the $NaNO_3$ used was above 99%.

The physical properties of Ga (Ref. 8) are also listed in Table 1. Semiconductor grade Ga of 99.9999% purity was used.

Samples of $NaNO_3$ and Ga were prepared for welding by melting and casting. The top and bottom surfaces were ground flat and cleaned before welding. The dimensions of the samples were 10 x 10 x 2 cm for $NaNO_3$ and 2.5 cm diameter by 1 cm height for Ga.

Welding and Pool Shape Measurement

Stationary welds were made with a defocused CO_2 laser beam, with Ar shielding to protect the pool surface from oxidation in the case of Ga. The CO_2 laser beam had a wavelength of 10.59 µm, power stability of ±5%, beam quality of $M^2 < 1.2$ and beam mode of TEM_{00} and 90% purity (better than 90% Gaussian), where M is the magnification factor. The beam divergence was 3.2 mR. The beam power was measured with a power meter having a 0.1-W resolution, and the beam diameter was measured with a micrometer-mounted device developed recently (Ref. 3).

The welding times were 3 min for $NaNO_3$ and 4 min for Ga. These were sufficient for the pools to stabilize in size. The melt was decanted from the pool immediately after the CO_2 laser was turned off. In fact, there was plenty of time for decanting. Solidification of the $NaNO_3$ melt did not start until about 5 s after the CO_2 laser was turned off because of the rather low thermal conductivity of $NaNO_3$ (Table 1). The Ga melt, on the other hand, just remained undercooled at room temperature (23°C) indefinitely, *i.e.*, for days.

The shape of the emptied pool was determined by using a digital x-y stage with a resolution of 0.01 mm and a fine-tip dial indicator with a resolution of 0.025 mm. The depth of the pool was measured every 0.25 mm along the diameter, in two directions perpendicular to each other, to determine the pool shape.

Table 1 — Physical Properties of $NaNO_3$ and Ga Melts (4–8)

Properties	$NaNO_3$	Ga
Melting point, T_m, °C	306.8	29.9
Heat of fusion, H, J/g	182	80
Temperature coefficient of surface tension, (γ/ T, dyne/(cm°C)	–0.056	–0.10
Surface tension, γ, dyne/cm	119.96 at T_m	718 at T_m
Dynamic viscosity, μ, g/(cm s)	0.0302 at T_m	0.0194 at T_m
Density, ρ, g/cm^3	1.904 at T_m	6.1 at T_m
Kinematic viscosity, $\upsilon = \mu/\rho$, cm^2/s	1.586×10^{-2} at T_m	3.18×10^{-3} at T_m
Specific heat, Cp, J/(g°C)	1.71 at T_m	0.398 at T_m
Thermal conductivity, k, W/(cm°C)	5.65×10^{-3} at T_m	0.33 at T_m
Thermal expansion coefficient, β, °C^{-1}	6.6×10^{-4}	9.2×10^{-5}
Thermal diffusivity, $\alpha = k/(\rho\ C_p)$, cm^2/s	1.74×10^{-3} at T_m	0.136 at T_m
Prandtl number, $Pr = C_p\mu/k$	9.12 at T_m	2.34×10^{-2} at T_m
Refractive index, n	1.46	
Emissivity, ε	0.3	
Transmission range, λ, cm	0.35×10^{-4}–3×10^{-4}	

Results

$NaNO_3$ Pool Shapes

The shapes of the $NaNO_3$ pools are shown in Figs. 2 and 3. At a low power of 4.5 W and a beam diameter of 3.2 mm, the pool is small and has a concave pool bottom, as shown in Fig. 2A. The depth/width ratio is 0.184. Herein, the width refers to the diameter of the pool surface and the depth refers to the pool depth along the pool axis.

As the power is raised to 12.4 W, the pools become much wider. At the beam diameter of 5.9 mm, the pool bottom is surprisingly flat, as shown in Fig. 2B. The depth/width ratio is 0.125.

As the beam diameter is reduced from 5.9 to 1.5 mm under the same power of 12.4 W, the depth at the pool center decreases while that near the pool edge increases. As shown in Fig. 2C, this results in a peculiar pool shape, shallower at the center and deeper near the pool edge. In other words, the pool bottom has become convex toward the melt. The depth/width ratio is only 0.096.

As the power is raised from 12.4 to

16.5 W, the pools become larger, but the characteristics of the pool shapes remain unchanged. At the beam diameter of 5.9 mm, the pool is flat at the bottom, as shown in Fig. 3A. The depth/width ratio is only 0.116.

As the beam diameter is reduced from 5.9 to 1.5 mm under the same power of 16.5 W, the pool bottom once again becomes convex, as shown in Fig. 3B. The depth/width ratio is 0.135.

Ga Pool Shape

The shapes of the Ga pools are shown in Figs. 4 and 5. They are significantly narrower and deeper than the wide and shallow $NaNO_3$ pools shown previously in Figs. 2B, 2C and 3.

At 7.5 W of power and a 5.9-mm beam diameter, the pool is concave, as shown in Fig. 4A. The depth/width ratio is 0.389.

As the beam diameter is reduced from 5.9 to 1.5 mm under the same power of 7.5 W, the pool becomes narrower and deeper to be nearly hemispherical, as shown in Fig. 4B. The depth/width ratio is 0.496.

As the power is raised to 15 W, the pools become larger, but the characteristics of the pool shapes remain unchanged. At the beam diameter of 5.9 mm, the pool is rather concave, as shown in Fig. 5A. The depth/width ratio is 0.413.

As the beam diameter is reduced from 5.9 to 1.5 mm under the same power of 15 W, the pool once again becomes nearly hemispherical, as shown in Fig. 5B. The depth/width ratio is 0.525.

Discussion

Peclet Number and Marangoni Number

The Peclet number Pe is defined as follows (Ref. 9):

$$Pe = \frac{LV}{\alpha} = \frac{LV\rho C_p}{k} = \frac{V\rho C_p \Delta T}{k\Delta T / L} = \frac{\text{heat transport by convection}}{\text{heat transport by conduction}} \quad (1)$$

where L is the characteristic length, V is the characteristic velocity, α is the thermal diffusivity (= $k/\rho C_p$), ρ is the density, C_p is the specific heat, k is the thermal conductivity and T is the temperature drop from the center to the edge of the pool surface.

The purpose of using Pe here is to discuss the effect of Marangoni convection on the shape of the weld pool in the absence of a surface-active agent. As such, the characteristic length L is taken as the radius of the pool surface and the characteristic velocity V as the maximum outward surface velocity at the pool surface. In contrast, a Peclet number, based on L = the pool depth and V = the maximum velocity in the pool, was used by Pitscheneder, *et al.* (Ref. 10), to explain the effect of sulfur on the shape of steel weld pools.

The Marangoni number, which is a measure of the extent of Marangoni convection, is defined as

$$Ma = \frac{-\frac{\partial \gamma}{\partial T}\left(\Delta T\right)L}{\mu\alpha} \quad (2)$$

where γ/ T is the temperature coefficient of surface tension, T is the temperature difference between the center and edge of the pool surface, L is the radius of the pool surface, μ is the dynamic viscosity and α is the thermal diffusivity.

When the power of the heat source is increased, T and L both increase and Ma increases. When the beam diameter is reduced, T increases very significantly, especially when the thermal conductivity is low (Ref. 3), and Ma increases very significantly. In any case, the higher Ma, the stronger Marangoni convection and the higher the maximum outward surface velocity V.

$NaNO_3$ Pools

For $NaNO_3$, the Peclet number is high for two reasons. First, the thermal conductivity k is very low (Table 1). Second, the outward maximum surface velocity V is significant and, in fact, can be rather high. Strong Marangoni convection has been observed recently by flow visualization in a simulated weld pool of $NaNO_3$ 10 mm in diameter, where Ma was around 2 x 10^4 (Ref. 3). Since the Peclet number is high, heat transport in a $NaNO_3$ pool is dominated by Marangoni convection.

At a low power of 4.5 W, the pool is still small (Fig. 2A) and the Peclet number, though not small, is not yet very high in view of the small pool size and mild convection.

As the power is raised to 12.4 W and the beam diameter changed to 5.9 mm, however, the pool becomes much wider (Fig. 2B) and Marangoni convection becomes significantly faster. Since L and V both increase, Pe increases significantly according to Equation 1. Marangoni convection dominates heat transport in the pool, and the strong outward surface flow carries heat from the laser beam to the pool edge. Since heat is transported to the pool edge more effectively and parallel to the pool surface, the resultant pool bottom is wide and flat.

Graphite powder, as a tracer to reveal convection, was introduced into the pool in a subsequent experiment. The maximum surface velocity was estimated to be about 2 cm/s from the videotape recording, based on the particle displacement measured and the 30 frames/s frame rate. From $\alpha = 1.74 \times 10^{-3}$ cm^2/s for $NaNO_3$, L = 5.8 mm (Fig. 2B) and Equation 1, Pe = 670. It is, therefore, evident Marangoni convection dominates heat transport in the pool. The error caused by the density difference between the

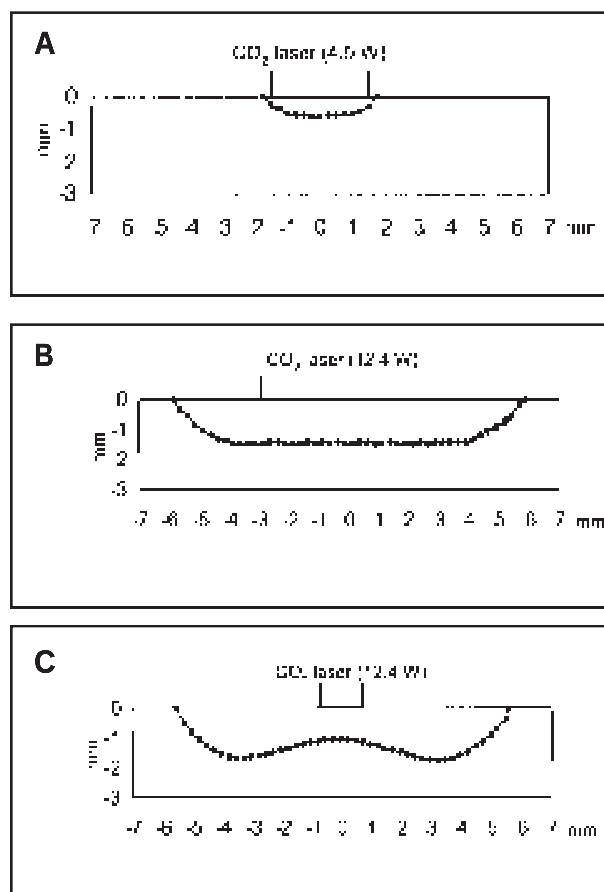

Fig. 2 — Shapes of stationary weld pools in $NaNO_3$ produced by CO_2 laser beams of the following: A — 4.5 W and 3.2 mm diameter; B — 12.4 W and 5.9 mm diameter; C — 12.4 W and 1.5 mm diameter.

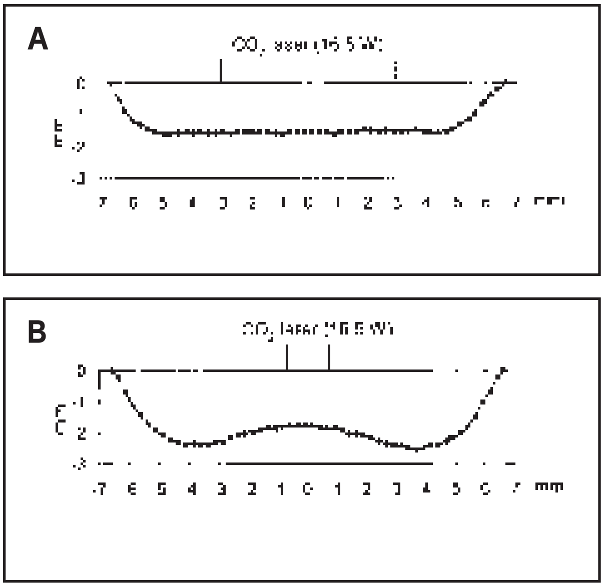

Fig. 3 — Shapes of stationary weld pools in $NaNO_3$ produced by CO_2 laser beams of the following: A — 16.5 W and 5.9 mm diameter; B — 16.5 W and 1.5 mm diameter.

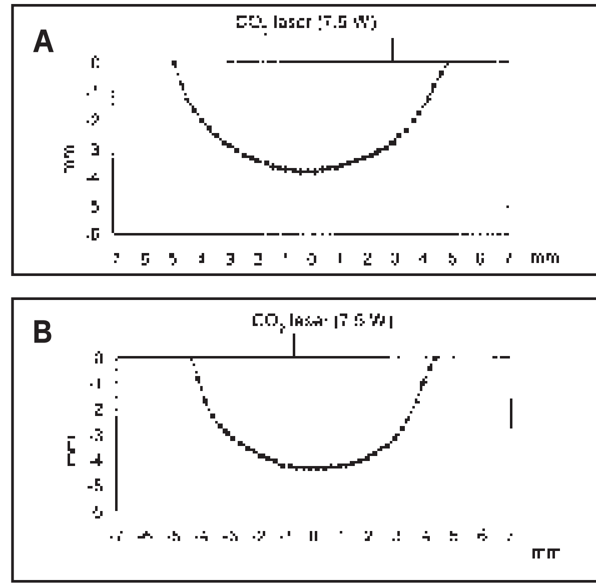

Fig. 4 — Shapes of stationary weld pools in Ga produced by CO_2 laser beams of the following: A — 7.5 W and 5.9 mm diameter; B — 7.5 W and 1.5 mm diameter.

graphite powder and the $NaNO_3$ melt is negligible, as described below.

From Strokes' law (Ref. 11)

$$v_s = \left(\frac{\mathbf{g} d_p^2}{18\upsilon_F}\right)\left\{\left(\frac{\rho_p}{\rho_F}\right) - 1\right\} \qquad (3)$$

where **g** is the gravitational acceleration (980 cm/s^2), d_p is the diameter of the graphite powder (0.020 cm), υ_F is the kinematic viscosity of the $NaNO_3$ melt (1.586 x 10^{-2} cm^2/s [Table 1]), ρ_p is the density of the graphite powder (1.77 g/cm^3 [Ref. 12]) and ρ_F is the density of the $NaNO_3$ melt (1.904 g/cm^3 [Table 1]). From Equation 3, the settling velocity of graphite powder in the $NaNO_3$ melt is 0.0967 cm/s upward, which is negligible as compared to the maximum surface velocity 2 cm/s.

The estimated maximum surface velocity, V, of 2 cm/s is apparently much lower than that in metal weld pools. It has been reported in laser beam and GTA welding of aluminum and steel that T is in the range 500–1050°C and that V is on the order of 1 m/s (Ref. 13–16). In the present study, L 3 mm but T is no greater than 73°C because no decomposition of $NaNO_3$ was observed during welding. The decomposition temperature 380°C (Table 1) is only 73°C above the melting point of 307°C. It is worth mentioning that a maximum surface velocity of about 1 cm/s has been reported in the study of Marangoni convection in $NaNO_3$ (Ref. 6).

As the beam diameter is reduced from 5.9 to 1.5 mm under the same power of 12.4 W, Marangoni convection becomes much faster, as illustrated previously in Fig. 1B. Since V increases further, Pe also increases further. This very strong Marangoni convection forces the return flow to penetrate deeper near the pool edge and carry heat downward to the pool bottom, resulting in a convex pool bottom — Fig. 2C.

Graphite powder was again introduced into a similar pool in a subsequent experiment, and the maximum surface velocity was roughly estimated to be at least 6 cm/s from the videotape recording. From α = 1.74 x 10^{-3} cm^2/s for $NaNO_3$, L = 5.5 mm and Equation 1, Pe = 1900. This very high Pe indicates Marangoni convection completely dominates heat transport in the pool.

Both the flat (Figs. 2B and 3A) and convex (Figs. 2C and 3B) are a clear indication that Marangoni convection dominates over gravity-induced buoyancy convection. The pool bottoms would have been concave if buoyancy convection had dominated in the pools.

Chan, *et al.* (Ref. 17), showed a convex pool bottom in the computer simulation of $NaNO_3$ welding with a moving rectangular laser beam. However, their Peclet number cannot be compared to that here since it was based on the scanning velocity of the laser beam rather than the maximum outward surface velocity, V.

Ga Pools

For Ga, on the other hand, the Peclet number is very low. First, its thermal conductivity k is very high (Table 1). Second, the maximum outward surface velocity V is expected to be rather small in view of the very small Ma, explained below.

A thermocouple was positioned below the center of the pool surface during the laser beam welding of Ga, and a very small T of only about 3°C was measured. This very small T is not just because the thermal conductivity is very high, but also because the melting point 29.9°C is almost identical to the room temperature (23°C). Consequently, to produce a 10-mm-diameter pool in the sample, only less than 10 W is needed. Without a large T to induce significant surface tension gradients along the pool surface, there is little Marangoni convection in the pool.

From Table 1, for Ga, γ/ T is –0.10 dyne cm^{-1}°C^{-1}, μ is 1.94 x 10^{-2} g cm^{-1}s^{-1} and α is 0.136 cm^2 s^{-1}. For a pool of 10 to 12 mm diameter, such as those shown in Figs. 4 and 5, L = 0.55 cm. As such, from Equation 2, Ma = 60, which is about three orders of magnitude lower than Ma = 2 x 10^4 for $NaNO_3$.

Since the Peclet number is very low, heat transport in a Ga pool is dominated by conduction. The downward as well as outward heat conduction results in a concave weld pool — Fig. 4A. As the beam size is reduced under the same power, the pool becomes nearly hemispherical. This further confirms that conduction dominates heat transport in the pool. According to the theory of conduction heat transfer, a weld pool should become hemispherical in shape as the heat source shrinks in size to a point at the center of the pool surface.

Peclet Number and Pool Shape

Based on the above discussion, it is proposed that the pool bottom can change from concave to flat and even convex as the Peclet number increases, as illustrated in Fig. 6. The weld pool can be either stationary or traveling with respect to the workpiece. In the latter case, however, the travel speed should be significantly less than V, which is usually the case, and V should be the maximum outward surface velocity in the *transverse* direction.

With Pe <<1, heat transport in the weld pool is dominated by conduction, and the pool is concave. The actual pool shape depends on the size of the heat source; with a small-size heat source, the pool is hemispherical, as illustrated in Fig. 6 (point A).

With Pe >>1, on the other hand, heat transport in the weld pool is dominated by convection, and the shape of the pool bottom can change from concave to flat or even convex, as illustrated in Fig. 6 (points B–D). With stronger convection carrying more heat to the pool edge, the pool bottom becomes flat — Fig. 6 (point C). When convection gets strong enough to also carry heat downward near the pool edge, the pool bottom becomes convex — Fig. 6 (point D). The smaller the thermal diffusivity, the more significant the effect of convection on the pool shape.

Welds in Materials of Various Prandtl Numbers

Figure 7 is a grid showing examples of welds with a hemispherical, concave, flat or convex bottom that have been observed in materials ranging from gallium and aluminum of very low Pr (~0.02) to $NaNO_3$ of very high Pr (~9). Heat transport in the weld pool ranges from "conduction highly dominating" in the bottom-left corner of the grid to "convection highly dominating" at the top and the right. These welds were made by laser beam welding (LBW), electron beam welding (EBW) or gas tungsten arc welding (GTAW), and will be called LB welds, EB welds and GTA welds, respectively. The LBW and EBW here refer to conduction-mode welding, in which the beam just deposits heat on the pool surface, as opposed to the case where the beam actually creates a vapor hole in the pool (the keyhole mode).

The interplay among many different factors determines weld pool convection. They include the power-density distribution of the heat source, the electromagnetic force in the pool, the arc plasma shear stress, the arc plasma pressure, the physical properties of the material and the surface-active agent. This interplay is sometimes too complex to analyze even with the help of computer simulation. However, in view of Fig. 7 and the observations made in the present study, it is clear that, for a given material composition and welding process, the weld shape often reveals a good deal about the nature of weld pool convection.

First, welds with a flat or convex bottom, as those in the top two rows of Fig. 7, suggest dominance of heat transport by outward surface flow induced either by Marangoni convection (in LBW and EBW) or by the arc plasma shear stress (in GTAW). Neither the electromagnetic force nor the surface-active agent plays a significant role.

Second, for metals with melting points close to the room temperature, conduction dominates heat transport in the weld pool. A more nearly hemispherical weld suggests a smaller heat source, as that in the bottom row of Fig. 7. The outward surface flow induced by Marangoni convection is too strong for commonly welded metals such as aluminum, steel and stainless steel to have a hemispherical pool. GTA, LB and EB welds of steel or stainless steel somewhat hemispherical in shape suggest dominance of heat transport by downward/inward convection induced either by the presence of a surface-active agent or by the electromagnetic force in the weld pool, or both.

Third, for commonly welded metals such as aluminum, steel and stainless steel without a surface-active agent, moderately concave welds, such as those shown in Figs. 7B, C and F, are common. Here outward surface flow induced by Marangoni convection is strong, but conduction still transports much heat down into the pool because of the low Pr.

The materials in Fig. 7 are discussed below.

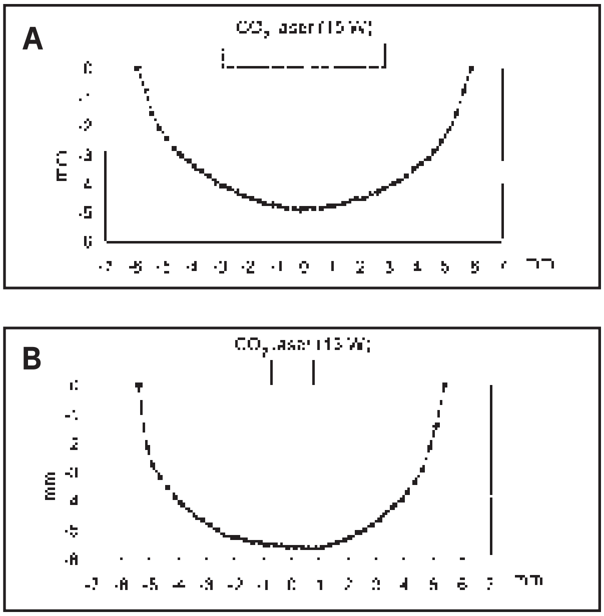

Fig. 5 — Shapes of stationary weld pools in Ga produced by CO_2 laser beams of the following: A — 15 W and 5.9 mm diameter; B — 15 W and 1.5 mm diameter.

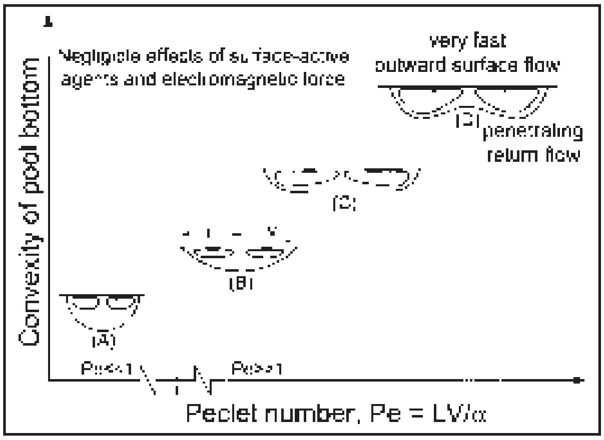

Fig. 6 — Proposed effect of Peclet number on weld pool shape. A — Conduction dominating (Pe << 1); B through D — convection dominating (Pe >> 1).

Gallium (Pr = 0.02)

The Ga weld shown in Fig. 7A is identical to that shown previously in Fig. 4B. As already mentioned, conduction dominates heat transport in the hemispherical pool of this weld.

Aluminum (Pr = 0.02)

Like Ga, the thermal conductivity of aluminum is very high. Unlike Ga, however, the melting point of aluminum, 660°C, is much higher than the room temperature, and substantial power is thus required for welding, *e.g.*, 1500 W

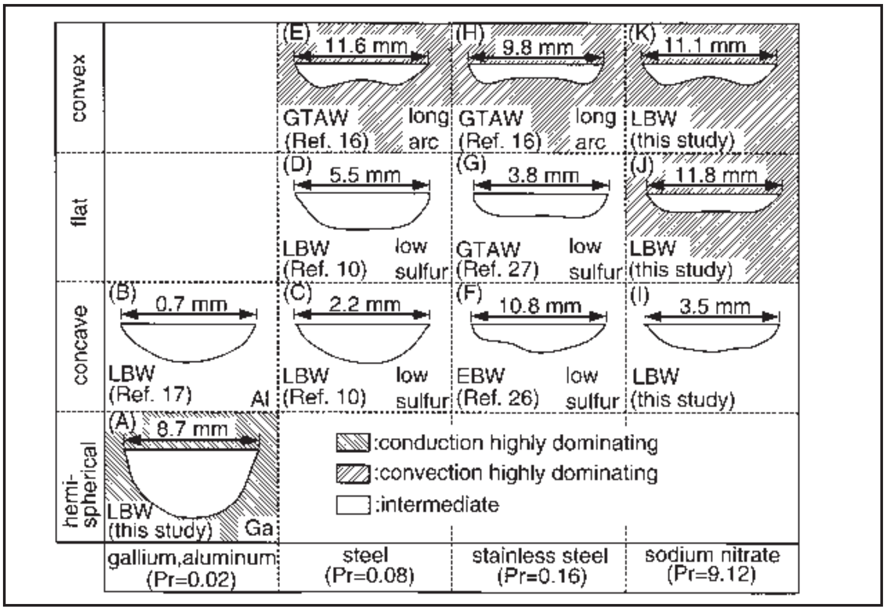

Fig. 7 — Welds of various shapes made in materials of various Prandtl numbers by GTAW, conduction-mode LBW or conduction-mode EBW. Ga and $NaNO_3$ represent the low and high extremes of Pr.

for GTAW, depending on the workpiece size. Considerable temperature gradients are thus present along the pool surface to induce strong Marangoni convection. Even so, the thermal conductivity of aluminum is so high that conduction always plays a very significant, if not dominating, role in heat transport. As such, aluminum welds made by GTAW, LBW or EBW are always concave but not hemispherical (Refs. 18–23). Figure 7B shows a concave bottom stationary weld in aluminum made by LBW (Ref. 18).

Even at very high Peclet numbers, an aluminum weld pool is still concave, rather than flat or convex. Although the outward surface flow greatly helps bring heat transport to the pool edge, this heat is still effectively dissipated by the highly conductive base metal instead of causing deeper melting at the pool edge like in steel or $NaNO_3$. From the computer simulation by Tsai and Kou (Ref. 24) for Marangoni convection in stationary conduction-mode laser beam welding of aluminum, a maximum surface velocity V of about 2 m/s is present in a concave weld pool of 6 mm diameter (L = 3 mm), based on $\alpha = 3.75 \times 10^{-1}$ cm^2/s for aluminum and Equation 1, Pe = 160. A similar Pe is obtained from the computer simulation by Kou and Sun (Ref. 16) for Marangoni convection in a concave stationary weld pool in gas tungsten arc welding of aluminum.

Steel (Pr = 0.08)

For steel, the thermal conductivity is significantly lower than that of aluminum. The pool bottom is concave but essentially flat, and even convex pool bottoms have been observed.

Figure 7C shows a concave bottom weld of a low-sulfur steel made by stationary LBW at 1900 W for 5 s (Ref. 10). The weld shown in Fig. 7D is a similar weld made under the same conditions except for the higher power of 5200 W. Pitscheneder, *et al.* (Ref. 10), have demonstrated by computer simulation that Pe is small (<1) for the 1900-W weld. For the 5200-W weld, however, Pe is much greater (about 40, considering their correction factor of 7 for k) because of the much higher maximum outward surface velocity of about 40 cm/s and the 2.5 times larger pool diameter.

Figure 7E shows a convex bottom weld of a mild steel made by stationary GTAW with a 8-mm-long arc (Ref. 25). With a long and, thus, wide arc, the electromagnetic force in the weld pool is reduced because the electric current field in the pool is not very diverging. The surface tension gradients are also reduced because the temperature gradients along the pool surface are reduced. On the contrary, the shear stress induced by the arc plasma acts on most of the pool surface instead of acting mainly near the center of the pool surface, as in the case of a short arc. Matsunawa, *et al.,* (Refs. 25, 26), have demonstrated by computer simulation the arc plasma shear stress outweighs both the electromagnetic force in the weld pool and the surface-tension gradients along the pool surface. The outward surface flow can be high enough (76 cm/s) to cause downward convection at the pool edge and hence a convex pool bottom. This effect of the outward surface flow on the shape of the pool bottom is exactly the same as that on the shape of the $NaNO_3$ pool bottom (Figs. 2C and 3B), even though the driving force is the arc plasma shear stress instead of the surface tension gradient. Since Pe is defined based on the maximum outward surface velocity V, the proposed effect of the value of Pe on the pool shape applies no matter whether the driving force is the arc plasma shear stress or the surface tension gradient.

Stainless Steel (Pr = 0.16)

For stainless steel, the thermal conductivity is even lower than that of steel, and the chance of a weld having an essentially flat bottom is even higher in stainless steel than in steel.

Figure 7F shows a concave bottom weld of a low-sulfur 304 stainless steel made by EBW (Ref. 27). The electromagnetic force in the pool is negligible because of the very low level of electric current used (75 mA).

Figure 7G shows a flat bottom weld of a low-sulfur 304 stainless steel made by GTAW (Ref. 28). Low-sulfur stainless steel welds with a flat bottom have been reported in LBW (Ref. 20) and EBW (Ref. 27), as well as GTAW (Refs. 27–29).

Figure 7H shows a convex bottom weld of a 77-ppm sulfur 304 stainless steel made by GTAW with an 8-mm-long arc (Ref. 25). As in the case of the convex bottom steel weld shown in Fig. 7E, Matsunawa, *et al.* (Refs. 25, 26), have shown by computer simulation the arc plasma shear stress outweighs both the electromagnetic force and the surface-tension gradients. A similar weld was obtained when the sulfur level was reduced to 18 ppm. With a 2-mm arc, however, the weld was much deeper in the 77-ppm sulfur material than in the 18-ppm sulfur material. These observations further support the conclusion that the outward surface flow induced by the plasma shear stress of the 8-mm arc dominates heat transport in the weld pool.

Sodium Nitrate (Pr = 9)

For $NaNO_3$, the thermal conductivity is very low and the weld pool bottom is usually flat or convex rather than concave.

The welds shown in Figs. 7I, J and K are identical to those shown previously in Figs. 2A, B and C, respectively. As already mentioned, Marangoni convection dominates heat transport in these welds.

Conclusions

1) A Peclet number has been defined as Pe = (pool radius L) x (maximum outward surface velocity V)/(thermal diffusivity α) to represent the ratio of (heat transport by convection)/(heat transport by conduction) in a weld pool. The outward surface flow referred to here can be induced either by the surface-tension gradients or the arc plasma shear stress along the pool surface.

2) For the weld pools of $NaNO_3$, a high-Pr material, Pe is easily very high because of the very low thermal diffusivity α and strong Marangoni convection (high V), and Marangoni convection highly dominates heat transport in the weld pool.

3) Increasing the beam power, which increases Marangoni convection and the pool size, increases V, L and, hence, Pe. The heat carried outward to the pool edge by the strong outward surface flow makes a concave pool bottom wide and flat. Reducing the beam diameter, which further increases Marangoni convection, further increases V and, hence, Pe. However, the return flow penetrates the pool bottom near the pool edge and makes the flat pool bottom convex. Both the flat and convex pool bottoms indicate Marangoni convection dominates over gravity-induced buoyancy convection in the pools.

4) For the weld pools of Ga, a low-melting-point and low-Pr material, Pe is very low because of the very high thermal diffusivity α and weak Marangoni convection (low V), and conduction dominates heat transport in the weld pool. Heat is conducted downward as well as outward, resulting in a concave pool bottom. Reducing the beam diameter makes the Ga pool more nearly hemispherical, further confirming conduction dominates heat transport in the pool.

5) It is proposed that, in the absence of both a surface-active agent and a significant electromagnetic force, a concave pool bottom can become flat or even convex as Pe increases to reflect increasing dominance of heat transport by the outward surface flow.

6) For a given material composition and welding process, the weld shape often reveals much about the nature of weld pool convection.

Acknowledgments

This work was supported by NASA under Grant No. NAG8-1459.

References

1. Heiple, C. R., and Roper, J. R. 1982. Mechanism for minor element effect on GTA fusion zone geometry. *Welding Journal* 61(4): 97-s to 102-s.

2. Ishizaki, K., Araki, N., and Murai, H. 1965. Penetration in arc welding and convection in molten metal. *Journal of Japan Welding Society* 34(2): 146–153 (in Japanese).

3. Limmaneevichitr, C., and Kou, S. Flow visualization of Marangoni convection in weld pools. *Welding Journal* 79(5): 126-s to 135-s.

4. White, L. R., and Davis, H. T. 1967. Thermal conductivity of molten alkali nitrates. *Journal of Chemical Physics* 47(12): 5433–5439.

5. Janz, G. J. 1972. *Journal of Physical Chemistry,* Reference Data 1(3): 583–704.

6. Preisser, F., Schwabe, D., and Scharmann, A. 1983. Steady and oscillatory thermocapillary convection in liquid columns with free cylindrical surface. *Journal of Fluid Mechanics* 126: 545–567.

7. Atomergic Chemetals Corporation. Datasheet. Farmingdale, N.Y.

8. Iida, T., and Guthrie, R. I. L. 1988. *The Physical Properties of Liquid Metals*, pp. 71, 92, 134, 183, 240. Oxford University Press, Oxford, England.

9. Bird, R. B., Stewart, W. E., and Lightfoot, E. N. 1960. *Transport Phenomena*, pp. 340–342. Wiley, New York, N.Y.

10. Pitscheneder, W., DebRoy, T., Mundra, K., and Ebner, R. 1996. Role of sulfur and processing variables on the temporal evolution of weld pool geometry during mutikilowatt laser beam welding of steel. *Welding Journal* 75(3): 71-s to 80-s.

11. Merzkirch, W. 1987. *Flow Visualization*, p. 44. Academic Press, Orlando, Fla.

12. Stackpole Carbon Division. 1986 Datasheet graphite grade 2020. St. Marys, Pa.

13. Oreper, G. M., and Szekely, J. 1984. Heat- and fluid-flow phenomena in weld pools. *Journal of Fluid Mechanics* 147: 53–79.

14. Pitscheneder, W., Ebner, R., DebRoy, T., and Mundra, K. 1996. Weld pool geometry during high power conduction mode carbon dioxide laser welding. *Trends in Welding Research*, eds. H. B. Smart, J. A. Johnson and S. A. David. ASM International, Materials Park, Ohio.

15. Kim, W. H., Fan, H. G., and Na, S. J. 1997. Effect of various driving forces on heat and mass transfer in arc welding. *Numerical Heat Transfer, Part A* 32: 633–652.

16. Kou, S., and Sun, D. K. 1985. Fluid flow and weld penetration in stationary arc welds. *Metallurgical Transactions A* 16A: 203–213.

17. Chan, C., Mazumder, J., and Chen, M. M. 1984. A two-dimensional transient model for convection in laser melted pool. *Metallurgical Transaction A* 16A: 2175.

18. Michaud, E. J., Kerr, H. W., and Weckman, D. C. 1996. Temporal pulse shaping and solidification cracking in laser welded Al-Cu alloys. *Trends in Welding Research*, eds. H. B. Smart, J. A. Johnson and S. A. David, pp. 153–158, ASM International, Materials Park, Ohio.

19. Wittig, J. E., and Milewski, J. O. 1993. Fusion zone microstructural characterization from pulsed and continuous Nd:YAG welds of 2024-T3 aluminum. *International Trends in Welding Science and Technology*, eds. S. A. David and J. M. Vitek, pp. 199–203, ASM International, Materials Park, Ohio.

20. Jellison, J. L., and Reicher, D. M. 1991. Experimental verification of physical model of pulsed laser welding. *Modeling of Casting, Welding and Advanced Solidification Processes V*, eds. M. Rappaz, M. R. Ozgu and K. W. Mahin, pp. 105–113. The Minerals, Metals and Materials Society, Warrendale, Pa.

21. Kou, S., and Le, Y. 1983. Three-dimensional heat flow and solidification during the autogenous GTA welding of aluminum plates. *Metallurgical Transactions A* 14A: 2245–2253.

22. Kou, S., and Wang, Y. H. 1986. Three-dimensional convection in laser melted pools. *Metallurgical Transactions A* 17A: 2265–2270.

23. Martukanitz, R. P. 1986. Modeling of the heat affected zone of aluminum arc welds. *Advances in Welding Science and Technology*, ed. S. A. David, pp. 193–201. ASM International, Materials Park, Ohio.

24. Tsai, M. C., and Kou, S. 1989. Marangoni convection in weld pools with a free surface. *Internal Journal for Numerical Methods in Fluids* 9: 1503 –1516.

25. Matsunawa, A., and Shinichiro, Y. 1990. Fluid flow and its effect on penetration shape in stationary arc welds. *Recent Trends in Welding Science and Technology*, eds. S. A. David and J. M. Vitek, pp. 31–35. ASM International, Materials Park, Ohio.

26. Matsunawa, A. 1993. Modeling of heat and fluid flow in arc welding. *International Trends in Welding Science and Technology*, eds. S. A. David and J. M. Vitek, pp. 3–16. ASM International, Materials Park, Ohio.

27. Pierce, S. W., Burgardt, P., and Olson, D. L. 1999. Thermocapillary and arc phenomena on stationary steel welding. *Welding Journal* 78(2): 45-s to 52-s.

28. Aidun, D. K., and Martin, S. A. 1997. *Journal of Materials Engineering and Performance* 6(4): 496–502.

29. Leinonen, J. I. 1995. Shielding gas selection for increased weld penetration and productivity in GTA welding. *Trends in Welding Research*, eds. H. B. Smart, J. A. Johnson and S. A. David, pp 353–357. ASM International, Materials Park, Ohio.